Published in final edited form as:
Microcirculation. 2010 April ; 17(3): 206–225. doi:10.1111/j.1549-8719.2010.00029.x.

Tumor Microvasculature and Microenvironment: Novel Insights Through Intravital Imaging in Pre-Clinical Models

Dai Fukumura, **Dan G. Duda**, **Lance L. Munn**, and **Rakesh K. Jain**
Edwin L. Steele Laboratory for Tumor Biology, Department of Radiation Oncology, Massachusetts General Hospital and Harvard Medical School, Boston, Massachusetts, USA

Abstract

Intravital imaging techniques have provided unprecedented insight into tumor microcirculation and microenvironment. For example, these techniques allowed quantitative evaluations of tumor blood vasculature to uncover its abnormal organization, structure and function (e.g., hyper-permeability, heterogeneous and compromised blood flow). Similarly, imaging of functional lymphatics has documented their absence inside tumors. These abnormalities result in elevated interstitial fluid pressure and hinder the delivery of therapeutic agents to tumors. In addition, they induce a hostile microenvironment characterized by hypoxia and acidosis, as documented by intravital imaging. The abnormal microenvironment further lowers the effectiveness of anti-tumor treatments such as radiation therapy and chemotherapy. In addition to these mechanistic insights, intravital imaging may also offer new opportunities to improve therapy. For example, tumor angiogenesis results in immature, dysfunctional vessels—primarily caused by an imbalance in production of pro- and anti-angiogenic factors by the tumors. Restoring the balance of pro- and anti-angiogenic signaling in tumors can "normalize" tumor vasculature and thus, improve its function, as demonstrated by intravital imaging studies in preclinical models and in cancer patients. Administration of cytotoxic therapy during periods of vascular normalization has the potential to enhance treatment efficacy.

Keywords

intravital microscopy; angiogenesis; lymphangiogenesis; tumor; stromal cells; micro-environment; vascular normalization

INTRODUCTION

The past three decades have witnessed spectacular advances in our understanding of the molecular origins of cancer and other diseases. These advances have led to the identification of various genes associated with carcinogenesis, tumor angiogenesis and other pathological processes, as well as to the development of a vast array of therapeutic agents. This has been possible through measurements of gene expression, physiological parameters and drug delivery that are typically measured with techniques which are either destructive or have poor spatial resolution (millimeter to centimeter). The former have limited ability to provide insight into the dynamic processes within tumors and the latter preclude the detection of

Address for correspondence: Dai Fukumura or Rakesh K. Jain, Edwin L. Steele Laboratory for Tumor Biology, Department of Radiation Oncology, Massachusetts General Hospital and Harvard Medical School, 100 Blossom Street – Cox 7, Boston, MA 02114, USA. dai@steele.mgh.harvard.edu or jain@steele.mgh.harvard.edu.

biological events that occur at the cellular and sub-cellular level and which require a resolution of 1–10 μm.

Intravital microscopy (IVM)—optical imaging of living organisms—can overcome these limitations. Indeed, IVM has provided unprecedented molecular, cellular, anatomical and functional insights into tumor pathophysiology including angiogenesis and the microenvironment [76]. Furthermore, the advent of reporters such as green fluorescent protein (GFP), as well as of transgenic mice and/or cell lines with these reporter gene constructs, has opened new avenues to investigate functional genomics. This review summarizes the use of imaging techniques in preclinical models for studies of tumor pathophysiology. Beyond the conceptual advances in tumor biology, these techniques are easily adapted to studies of normal tissue or other diseases, and some of them have the potential to be useful in the clinic.

INTRAVITAL MICROSCOPY TECHNIQUES

Studies of tumor angiogenesis, vascular function and microenvironment are being pursued using multiple approaches. For example, histological and molecular methods readily provide quantitative analyses at tissue, cellular, sub-cellular and molecular levels in both preclinical models and in clinical studies. However, these techniques are not suitable for dynamic or functional studies and are highly invasive. On the other hand, imaging techniques provide non-invasive or minimally invasive dynamic measurements of physiological functions in real-time. Despite major advances in clinical imaging techniques such as PET, CT, and MRI, their spatial resolution remains insufficient for visualization of cellular and sub-cellular events [151]. IVM imaging in combination with sophisticated genetic models and animal preparations (e.g., window models) can overcome some of these limitations in preclinical tumor models.

Four essential components are required to perform quantitative IVM: (i) tissue preparations that permit optical access; (ii) molecular probes that can be detected by a microscope; (iii) a microscope and detection system; and (iv) computer algorithms and mathematical models that can extract parameters of interest from the image data set (Figure 1A). There are three different kinds of tissue preparations for IVM: (i) *in situ* preparations; (ii) acute (exteriorized) tissue preparations; and (iii) chronic-transparent windows. *In situ* preparations such as ear and tail models do not require any invasive preparation [54,62,113]. However, the depth accessible by this technique is limited. Acute exteriorization models such as those used for mammary pad [28,111,159,161] and liver [46,104] could be applied to virtually any tissue, with variable degrees of difficulty. However, the duration and frequency of the observation is limited and the preparation procedures may affect the physiological parameters. Chronic window models such as dorsal skinfold chamber [97], mammary fat pad chamber [137,148] and cranial window [166] require surgical implantation and sufficient recovery time after the implantation, but permit repetitive observation thereafter. Lifetimes of these windows vary and depend on their location and the tumor implant type, but range from 3–4 weeks (dorsal windows) to several months (cranial window). Once the tissue preparation is ready for observation, the animal is transferred to the specially designed microscope stage and the tissue is visualized using an appropriate exogenous or endogenous molecular probe depending on the parameter(s) of interest (Table. 1).

Achieving high resolution using conventional light microscopy comes at the expense of diminished depth penetration. Light scattering and signal absorption within tissues limit access of typical epifluorescence and confocal laser-scanning microscopy to approximately 100 μm into the tissue. The multiphoton laser-scanning microscope has significantly improved depth penetration in tissues and, in combination with chronic window models,

allows repetitive imaging at depths of several hundred micrometers within living tissue while retaining sub-micrometer spatial resolution [9]. Another important development is the development of newer and brighter probes (e.g., quantum dots) to probe tumor environment [132,135]. Most recently, optical frequency domain imaging (OFDI), a second generation of optical coherence tomography (OCT), has emerged as a robust high volumetric imaging technique with sufficiently high resolution (10 μm) to study blood and lymph vessels. OFDI has markedly superior depth penetration and allows repetitive imaging at depths of several millimeters [148].

Conventional Intravital Single-Photon Microscopy

The standard microscopy workstation consists of an upright or inverted microscope equipped with trans-illumination and fluorescence epiillumination, a flash-lamp excitation device, a set of fluorescence filters, a motor-controlled filter wheel, a CCD camera, a video monitor, a video recorder and a frame grabber board for image digitization (Figure 1A). Advanced techniques require additional equipment such as a motorized X–Y stage with ±1.0-μm lateral resolution, an intensified CCD camera, a photomultiplier tube and a dual-trace digital oscilloscope.

Intravital Multiphoton Laser-Scanning Microscopy

An intravital multiphoton laser-scanning microscopy (MPLSM) consists of a mode-locked Ti:Sapphire laser and a laser scan-head that can be purchased either as part of a MPLSM system or as a confocal system with further modifications enable infra-red transmission. The laser beam first passes through a Pockels Cell—which allows rapid (~1 ms) modulation of laser intensity—and then is directed by the scan-head into the side- or top-entry port of an upright epifluorescence microscope. Non-descanned photomultiplier tubes are used for imaging through significant depths of scattering tissue and should be introduced into the beam path via a dichroic beam splitter located in the beam path between the scan-head and the objective lens [9,72].

To measure tumor size using MPLSM (or single photon microscopy), we need low magnification images. To quantify physiological parameters, randomly selected areas (3–6 locations/tumor or animal) are investigated using long working distance objectives with appropriate magnification. The parameters that can be routinely measured include: angiogenesis (vascular density, length, diameter, etc.) [9,97]; hemodynamics (e.g., erythrocyte velocity) [9,31]; vascular permeability [9,48,164]; vessel pore cutoff size [60]; leukocyte–endothelial interaction [9,41,131]; lymphangiogenesis and lymphatic function [62,96]; interstitial diffusion and convection by fluorescence photobleaching with spatial Fourier analysis [5,11]; tissue oxygen level by phosphorescence quenching [59,144], tissue pH by fluorescence ratio imaging [18,59]; localization and activity of gene expression by fluorescent reporter imaging [9,43]; and fibrillar collagen structure and dynamics by second harmonic generation imaging [11,124].

Intravital Optical Frequency Domain Imaging

To circumvent the technical limitations of fluorescence microscopy, we recently implemented OFDI for intravital imaging of tumors. OFDI can provide unprecedented access to previously unexplored, critically important aspects of tissue biology (Figure 1B and Figure 3A). For example OFDI can be used to quantify tumor angiogenesis and lymphangiogenesis.

The inner workings of this instrumentation have been recently published [148]. In brief, OFDI provides high-resolution imaging of the elastic light scattering properties of a sample in 3-D. Interferometric measurements first sample in parallel the interference signal between

light scattered at all detectable depths and an external reference beam as a function of wavelength. Fourier analysis of this interference signal across wavelength separates the combined signals across all depths into a depth-resolved scattering profile. Volumetric datasets describing the structural features of the tissue are generated from the sum of the magnitude of the reflected field in each of the detected polarization states. The magnitudes (dB scale) are mapped to grayscale for display. Presentations of the structure use mean projections over small extents in the dimension out-of-plane of the image to reduce speckle noise and enhance contrast.

We used Doppler-OFDI to image in a short period of time (~10 min) entire tumors (4 mm × 5 mm) in 3D. The depth resolution for this technique is 5 μm and the axial resolution is approximately 10 μm. Because the scattered signal that is used to create images is based upon intrinsic motion of the circulating red blood cells (RBCs), no external contrast agent is necessary. On the other hand, OFDI cannot visualize fluorescent probes. Thus, OFDI technology will have to be used in conjunction with MPLSM to address certain biological questions.

INTRAVITAL MICROSCOPY STUDIES OF TUMOR MICROVASCULATURE

Abnormal Blood Vessel Networks in Tumors

IVM is commonly used to determine the size and architecture of tumors and their vasculature. RBCs can be used as an endogenous contrast agent to visualize blood vessels under conventional trans-illumination, linearly polarized light [52], OCT [139] or OFDI [148] (Figure 1B). High-molecular-weight fluorescent tracers (e.g., FITC-conjugated 2000 kDa dextran) are injected to temporarily demarcate the blood vessels for fluorescence microscopy until the extravasation of the tracers degrades contrast. This technique allows dynamic measurement of vessel diameter, length, surface area and volume, branching patterns and intercapillary distance in growing or regressing tumors [162,166]. IVM studies have characterized normal vascular networks, which consist of differentiated units such as arterioles, capillaries and venules, and form a well-organized architecture with dichotomous branching and hierarchic order (Figure 1C). In contrast, tumor vessels are dilated, saccular, tortuous, and heterogeneous in their spatial distribution (Figure 1C) [68]. Tumor vasculature is disorganized and has trifurcations and branches with uneven diameters. Fractal analysis of IVM images of normal and tumor vascular networks reveals that the former are optimally designed to provide nutrients by diffusion to all normal cells (so-called diffusion-limited aggregation), whereas the latter are restricted by the mechanical properties of the matrix (called invasion percolation) [2,47]. The molecular mechanisms causing these abnormal vascular architectures are not completely understood, but a key contributor is considered to be the imbalance of pro- and anti-angiogenic factors in the tumor tissue [71]. Another potential factor is the solid (mechanical) stress that is generated by proliferating tumor cells, which can compress blood vessels and lymphatics [121,128].

Abnormal Blood Flow in Tumors

Furthermore, RBC velocity measurements by IVM revealed spatially and temporally heterogeneous blood perfusion in tumors [9,41,45,46,68,97,165]. Overall perfusion rates (blood flow rate per unit volume) in many tumors are lower than those in many normal tissues and the average RBC velocity in tumor vessels can be an order of magnitude lower than in normal vessels [9,97,166]. Unlike normal vessels, there is no relationship between size of blood vessel and RBC velocity in tumors. Arterio-venous pressure difference and flow resistance govern blood flow in a vascular network. Flow resistance is a function of geometric (vascular architecture) and viscous (blood viscosity, rheology) resistances. Abnormalities in both vasculature and viscosity increase the resistance to blood flow in

tumors [25,68]. Focal leaks, which often exist in some of the tumor vessels, may also compromise the downstream blood flow. The heterogeneity of tumor blood flow hinders the delivery of therapeutic agents to tumors and causes abnormal microenvironment in tumors. The latter, in turn, compromises the effectiveness of various therapies, and selects for more aggressive and metastatic cancer cells.

Abnormal Leukocyte--Endothelial Interactions in Tumors

IVM observations also reveal that leukocyte–endothelial interactions are generally low and heterogeneous in tumor vessels [41,45,46,75,77,118,157]. IVM studies of adoptively transferred lymphocytes (after their prior labeling with a fluorescent dye) showed that activated lymphocytes adhere only to some tumor vessels but not to others [110,131]. These heterogeneous leukocyte–endothelial interactions may reflect heterogeneous expression of adhesion molecules on tumor vessels. Local imbalance of angiogenic factor signaling may also contribute to these heterogeneities. For example, vascular endothelial growth factor (VEGF) upregulates various adhesion molecules (including ICAM-1, VCAM-1, and E-selectin), whereas bFGF and Ang-1 down-regulate adhesion molecule expression in vascular endothelial cells [88,109,167]. The link between angiogenesis (VEGF) and inflammation (leukocyte adhesion) has also been shown in a number of *in vivo* models [20]. IVM will play a major role in deciphering the mechanisms by which these abnormal leukocyte–endothelial interactions contribute to abnormal immune responses in tumors [7,28,123].

Abnormal Vessel Structure in Tumors

The structure of vessel wall is also abnormal in tumors [14,108,142]. Large inter-endothelial junctions, increased numbers of fenestrations, vesicles and vesico-vacuolar channels, and a lack of normal basement membrane are often found in tumor vessels [27,156]. Perivascular cells have abnormal morphology and heterogeneous association with tumor vessels. In agreement with these structural alterations in the tumor vessel wall, time–course IVM monitoring of fluorescent macromolecules within blood vessels and interstitum demonstrated higher permeability in solid tumor vessels than that in most normal vessels [48,60,164]. Extravasation of molecules from the bloodstream occurs by diffusion, convection, and, to some extent, by transcytosis in an exchange vessel. Diffusion is considered to be the major form of transvascular transport in tumors [101]. The diffusive permeability of a molecule depends on its size, shape, charge, and flexibility as well as the transvascular transport pathway. For example, determination by IVM of vascular permeability to various sizes of fluorescently labeled macromolecules showed inverse relationship between molecular size and permeability [163].

Owing to physical limitations of optical microscopy, it is not possible to directly measure the dimensions of sub-micron structures *in vivo*. Instead, monitoring the movement of fluorescent nanoparticles in the tissue can provide such information. By titrating the extravasation of nanoparticles of increasing size, we found that the cut-off size of “pores” in the walls of tumor vessels varied from ~100 nm to 2 μm depending on the tumor type, the location of its growth and whether it is growing or regressing [60,112]. The large pore size —characteristic of most tumor vessels—leads to a lack of permselectivity (i.e., the property of the vasculature that allows only molecules of a certain size to cross the endothelial barrier) [163].

Unfortunately, the biggest challenge in transvascular transport in tumors stems from the spatial and temporal heterogeneity in permeability [112,163], which restricts access to some regions of tumors. However, it is possible to lower the vascular permeability of a tumor by blocking VEGF signaling [82,162]. Indeed, anti-angiogenic therapy alleviates vascular

hyperpermeability-associated abnormalities such as high interstitial fluid pressure (IFP) and brain vasogenic edema in cancer patients [3,83,154] (see section below).

Abnormal Lymphatic Vessels in Tumors

Fluorescence micro-lymphangiography has provided valuable information on pathophysiology of lymphatic vasculature in and around tumors [62,95,96,119]. Moreover, OFDI allows non-invasive tracer-free lymphangiography and monitoring of lymphatic vessels throughout tumor progression [148]. Furthermore, OFDI lymphangiography (negative contrast) can be performed simultaneously with OFDI angiography (positive contrast); the two techniques differ only in the methods for post-processing of the OFDI data.

Normal lymphatic capillaries collect excess fluid and macromolecules from tissues, and bring them back to the thoracic duct. By means of two different IVM methods, fluid velocity in the lymphatic capillaries was found to be ~1 to 10 μm/s—considerably faster than the interstitial fluid velocity (~0.1 μm/s), but slower than blood velocity (~100 to 1000 μm/s) [4,96,136]. Lymphatics in the *tumor margin* are hyperplastic, similar to those in the skin of mice engineered to overexpress VEGF-C, a lymphangiogenic growth factor, in their keratinocytes [80,95,119,148]. The diameters of these lymphatics in the tumor margin increase even further in tumors that overexpress VEGF-C [79,119]. However, overexpression of VEGF-C does not induce formation of functional lymphatics *within these tumors*. This is due to the compression of intra-tumor lymphatic vessels by mechanical stress (solid stress) created by tumor cell proliferation in a confined space [121]. As a result, there are no functional lymphatic vessels inside solid tumors [95,119]. Even if the structures with lymphatic endothelial markers are present in tumors, they do not transport fluid or macromolecules. The lack of functional lymphatics within tumors is a key contributor to the interstitial hypertension measured in animal and human tumors [69,74,95,119]. In contrast to the lack of functional intra-tumor lymphatics, functional lymphatic vessels are present in the tumor margin and the peri-tumoral tissue [62,119]. These peri-tumoral lymphatic vessels are hyperplastic and collect fluid, growth factors and cells exiting from tumors. In addition to these structural and functional parameters, IVM can be used to study lymph node metastasis. Detection of GFP-labeled metastatic tumor cells in peri-tumor lymphatics and monitoring their arrival into the nearby lymph node has demonstrated that the hyperplastic lymphatics in the tumor margin mediate metastasis [62].

INTRAVITAL MICROSCOPY STUDIES OF TUMOR MICROENVIRONMENT

Imaging Abnormal Metabolic Environment in Tumors

To monitor the metabolic microenvironment in tumors, IVM can be modified to utilize molecular probes that change their optical properties as a function of pO_2 and pH [59]. Hypoxia and acidosis are the hallmarks of abnormal metabolic environment in solid tumors (Figure 1D) [56,59,138]. Structurally and functionally abnormal tumor vessels fail to supply adequate amounts of nutrients and oxygen to tumors and to carry away acidic metabolites. Spatially heterogeneous angiogenesis and tumor growth generate hypovascular regions in tumors. These regions—localized far from blood vessels—become chronically hypoxic and acidic. Furthermore, blood flow in tumor vessels is temporally heterogeneous and thus, the intermittent blood flow causes periodic (acute) hypoxia in tumors [10,21]. Even the presence of blood flow does not guarantee the delivery of oxygen in solid tumors. High-resolution IVM revealed that some of the perfused tumor vessels carry almost no oxygen and there is no clear relationship between blood flow rate and oxygen tension (pO_2) of individual tumor vessels [59]. Moreover, simultaneous high-resolution mapping of tissue pO_2 (by phosphorescence quenching IVM) and pH (by fluorescence ratio-imaging IVM) revealed

that there is a lack of spatial correlation among these parameters [59]. These findings have significant implications since both pO_2 and pH are important determinants of tumor growth, metabolism, and response to a variety of therapies [8,145].

In addition, treatment with radiation therapy and many chemotherapeutic agents damages DNA by generating free radicals in the presence of oxygen [8,145]. Thus, hypoxia in solid tumors may significantly reduce sensitivity to treatments with radiation and these drugs. Since intracellular pH is neutral, acidic extracellular pH decreases the cellular uptake of weakly basic drugs [145]. Hypoxia and/or acidosis also compromise the function of immune cells targeting tumors and reduce the efficacy of host immune response and cell-based therapies. The hostile metabolic environment in tumors may select for tumor cells that are more aggressive and genetically unstable. These more malignant tumor cells are less susceptible to apoptosis, resistant to various therapies, and highly invasive and metastatic [32,122,127]. Finally, both hypoxia and acidic pH can induce various growth factors including VEGF and thus, contribute to tumor angiogenesis, growth and metastasis [37].

Imaging Angiogenesis Regulation by Metabolic Microenvironment

The discovery and commercial availability of live fluorescent reporters such as blue, cyan, green, yellow, red and far-red fluorescent proteins (BFP, CFP, GFP, YFP, DsRed and HcRed) have allowed IVM studies of gene expression and regulation. Transgenic cell lines or animals can be constructed using these fluorescent protein genes as reporters driven by the promoter of the gene of interest. In this manner, it has become possible to simultaneously monitor promoter activity along with measurement of microenvironmental factors known to regulate this activity, e.g., promotion of VEGF expression by hypoxia [43,44].

Hypoxia upregulates various angiogenic growth factors, including VEGF, angiopoietin (Ang) 2, platelet-derived growth factor (PDGF), placenta growth factor, transforming growth factor α, interleukin (IL)-8, and hepatocyte growth factor *in vitro* [56]. Low extracellular pH also causes stress-induced alteration of gene expression, including the upregulation of VEGF and IL-8 in tumor cells *in vitro* [160]. Despite its importance, the effect of the low and heterogeneous interstitial pO_2 and pH on VEGF expression *in vivo* remained unknown for many years due to the lack of appropriate techniques and animal models. The combination of fluorescence ratio imaging microscopy for pH measurements [105], phosphorescence quenching microscopy for pO_2 measurements [144] and the transgenic technology for visualization of VEGF promoter activity [43] has allowed the coordinated study of pH, pO_2, and VEGF expression *in vivo* (Figure 2A) [44]. Detailed analysis indicated that in low pH or oxygenated regions, tissue pH, but not pO_2, regulates VEGF promoter activity. Conversely, in hypoxic or neutral pH regions, tissue pO_2 and not pH regulates VEGF expression [44]. Tissue pO_2 and pH appeared to regulate VEGF transcription in tumors independently. In fact, the analysis of the VEGF promoter region revealed that acidic pH induces VEGF expression via Ras-ERK1/2-AP1 pathway but not the hypoxia inducible factor or hypoxia responsive element mediated pathway [160]. This example illustrates the insights that can be gained by fluorescence IVM into the role of the abnormal microenvironment in tumors.

Intravital Microscopy Studies of the Role of Host Stromal Cells in Tumor Angiogenesis

It is becoming increasingly accepted that tumor development and pathophysiology cannot be explained solely by the genetic modifications in malignant cells [149]. Host stromal cells profoundly influence many steps of tumor progression, such as angiogenesis, tumor cell proliferation, invasion, metastasis, and even malignant transformation [29,43,99,103,125,129,141].Interactions between the diverse cell types within a tumor, via

both soluble factors and direct cell-to-cell contact, play an important role in the induction, selection, and expansion of the neoplastic cells. “Successful” malignant cells are those that have acquired the ability to co-opt their normal neighbors by inducing them to release abundant growth-stimulating signals [99,141,149].

IVM observation of tumors grown in transgenic mice that express GFP in activated fibroblasts showed that VEGF promoter activity is strongest at the host–tumor interface [43] (Figure 2B). Furthermore, MPLSM showed that stromal cells with activated VEGF promoter associate with and surround tumor blood vessels inside the tumor [9] (Figure 2B). These findings indicate that activated fibroblasts are active participants in angiogenesis, fortify the newly formed vessels, and regulate their function. For example, stromal cells can produce approximately one-half of the VEGF expressed in teratomas [147]. Consistent with this conclusion, VEGF-null teratomas had about half the level of angiogenic activity compared with the wild-type tumors. The ratio of tumor-to-host-derived VEGF and other growth factors may vary depending on tumor type, stage, and organ site. For example, IVM studies showed higher VEGF activity in fibroblasts and higher vascular densities in advanced orthotopic tumors compared to early stage orthotopic or ectopic (subcutaneous) tumors [146].

Imaging Regulation of Angiogenesis and Vessel Function by Organ Microenvironment

IVM observation of the same tumors grown in different organ sites (windows) revealed organ sitedependent angiogenic activity and vessel function [35,76]. For example, B16 murine melanomas grown in a cranial window (a metastasis site) have higher vessel density and branching, and relatively smaller vessel size than those in the same tumors grown in a dorsal skin chamber (primary site) (Figure 2C,D) [84]. Similarly, human gliomas grown orthotopically (in cranial window) show a partial maintenance of the blood–brain barrier function while vessels of the same tumor grown subcutaneously (in dorsal skin chamber) are highly leaky [70]. In addition, the sizes of fluorescently labeled nanoparticles that extravasate across the blood vessel wall are smaller in tumors grown in brain microenvironment compared with the same tumors grown subcutaneously [60]. Organ-specific expression of pro-angiogenic and vessel maturation factors may contribute to differential angiogenic activities and vessel functions. For example, B16 melanomas exhibit higher levels of nitric oxide (NO) when grown in the brain compared with B16 tumors grown subcutaneously (Figure 2C) [84]. NO is a gaseous mediator involved in many biological processes including angiogenesis [40]. The highly metastatic variant of B16 (B16F10) produces more NO and exhibits higher angiogenic activity than that in low metastatic B16 variant (B16F1) (Figure 2D) [84]. These differences persist when the variants are gown in different organ microenvironments (i.e., brain versus subcutaneous space) [84] (Figure 2C). Another example is the difference between liver and subcutaneous microenvironment. IVM studies showed lower vessel densities in colon cancers and melanomas grown in the liver than those grown subcutaneously [46,53]. Correspondingly, the levels of VEGF and IL-8 mRNA in colon cancers and melanomas are lower when grown in the liver versus subcutaneously. Finally, IVM can be used to study the function of endogenous anti-angiogenic soluble factors. IVM observation of bFGF-containing gels in cranial windows revealed that mice bearing orthotopically grown human gallbladder tumors —but not those carrying ectopic subcutaneous tumors—exhibit anti-angiogenic activity in the cranial window-implanted gels [50].

In addition to regulation of pro- or anti-angiogenic factor expression, host–tumor interactions can also govern vascular response to a given stimulus. For example, IVM studies of gels containing the same dose of pro-angiogenic factors such as VEGF showed significantly more angiogenesis when implanted in cranial windows versus dorsal skin chambers [19]. In addition to inducing angiogenesis, VEGF is a potent vascular permeability

factor. Interestingly, a significantly higher amount of VEGF was required to induce vascular hyperpermeability in normal vessels of the brain than in those of the dorsal skin, presumably because of the blood–brain barrier [112]. Similar differences were seen for comparisons of tumors grown in the liver, mammary pad or subcutaneously. Angiogenesis and VEGF levels were enhanced in LS174T human colon cancers grown subcutaneously versus intra-hepatically. On the other hand, vascular permeability was higher when LS174T tumors were grown in the liver versus the subcutaneous space, presumably because of the fenestrations of liver sinusoidal vasculature [46]. Finally, higher VEGF expression and permeability but less angiogenesis were observed in ZR75 human breast cancers grown in the mammary fat pad (primary site) compared with those grown in the cranial window (metastatic site) [111]. The underpinnings of these organ-specific pathophysiological features revealed by IVM remain unclear. Future studies should investigate the roles of organ-specific endothelial cells, cell–cell and cell–matrix interactions, and the local microenvironment.

TRANSLATIONAL VALUE OF IVM STUDIES OF TUMORS

Tumor Response to Anti-Angiogenic Therapies: Role of Vascular Normalization

Various parameters obtained through IVM measurements can provide mechanistic and integrated insights in the response of tumor vessels to anti-angiogenic agents. These insights have led to new strategies for improving cancer detection and treatment. Anti-angiogenic therapy has been developed with the goal of destabilizing tumor vasculature to “starve” tumors. Unfortunately, while this goal has been achieved in pre-clinical models, the currently available agents failed to control tumor growth by anti-vascular effects [73]. On the other hand, restoring the balance between pro- and antiangiogenic factors by targeting pro-angiogenic signaling pathways may reverse the abnormalities of the vasculature and microenvironment. In turn, this may lead to a “normalized” function of the tumor vasculature [38,71]. Consistent with this notion, IVM studies revealed that various direct and indirect anti-angiogenic therapies can decrease tumor vessel diameter, reduce tortuosity and decrease fractal dimension toward the diffusion-limited aggregation regime [2,67,78,82,162]. In addition, as demonstrated by IVM, the anti-VEGF treatments reduce the size and length as well as permeability of abnormally dilated and tortuous tumor vessels (Figure 3A) [143,148,156,162]. Similarly, IVM studies of HER2+ breast cancers treated with indirect anti-angiogenic agents such as trastuzumab (an anti-human HER 2 antibody) showed vascular changes consistent with vascular normalization [67]. These changes contributed to normalization of both vasculature and microenvironment in tumors. Anti-VEGF treatments decreased tumor IFP in breast, colon cancers and gliomas [64,93,143] and improved tumor tissue oxygenation [93,156].

Counter-intuitively, normalization of the vasculature and microenvironment in tumors may indirectly benefit cancer patients. First, cytotoxic agents administered within the period of vascular normalization may show improved tumor penetration and efficacy. Decreased IFP restores pressure gradient across blood vessel wall as well as tumor interstitium and thus, increases drug penetration in tumors [79,143,153]. As a result of improved oxygenation, the efficacy of radiation treatments is significantly improved when delivered during the vascular “normalization window” after anti-VEGF therapy [92,93,156]. Second, vascular normalization after anti-VEGF therapy may decrease tumor vascular permeability and vasogenic edema, which may itself provide a benefit. For example, in the case of brain tumors, IVM studies in mice with orthotopically implanted human gliomas showed that mouse survival was increased despite persistent tumor growth after anti-VEGF therapy [83]. Third, normalization of the tumor vasculature and microenvironment could lead to improvement of the anti-tumor immune responses of the host or after adoptive transfer of activated lymphocytes [55].

Importantly, emerging evidence from clinical studies support some of these pre-clinical findings. For example, bevacizumab (an anti-human VEGF antibody) can decrease tumor IFP in rectal cancer patients [154,155], and its combination with cyto-toxics has shown synergistic effects in colorectal and lung cancers [49,65,130]. In brain and liver cancer patients, anti-VEGF therapy decreased vascular permeability, which correlated with improved survival outcomes [3,133,169].

IVM can also be used to uncover the cellular and molecular underpinnings of vascular normalization. For example, we determined the tissue distribution of signaling molecules such as nitric oxide (NO), a gaseous molecule that mediates angiogenesis and vessel maturation [40,84]. To this end, we used a molecular probe that changes its optical properties as a function of NO concentration. Imaging of the NO-sensitive fluorescent tracer revealed a lack of tissue gradient of NO in U87 human gliomas (Figure 3B). Restoration of the perivascular NO gradient normalized tumor vasculature, resulted in improved tissue oxygenation, and enhanced tumor response to radiation treatment (Figure 3C) [85]. It would be of great interest to use imaging to further characterize the roles of other factors linked to vascular normalization in genetic models, e.g., myeloid cells, endothelial PHD2, perivascular cell RGS5 or PDGFRβ [51,55,107,134]. Combining various agents—which normalize vasculature through different mechanisms—may produce even greater improvement in therapeutic outcomes.

FUTURE PERSPECTIVES

IVM has provided unique insights into angiogenesis and tumor biology [12,34,36,71,86]. Recent progress in optical technologies, probes and animal models are beginning to resolve several key limitations of IVM. Currently, the most widely used microscopy techniques are surface-weighted. Ideally, we should be able to study functional parameters inside tumors because these are both temporally and spatially heterogeneous. The use of MPLSM *in vivo* was a major breakthrough given its superior depth penetration, but it is not capable of imaging entire tumors [9,57,90,94]. The OCT-based OFDI is a novel optical method that enables dynamic observations of tissues for several millimeters in all three dimensions with high spatial resolution. Thus, OFDI can be used to image whole tumors in mice, to provide complementary structural and functional information to fluorescence IVM studies [148].

Image acquisition rate and speed of imaging are also improving [33,87,116]. High-speed imaging is necessary to capture dynamic events such as blood flow, leukocyte–endothelial interactions, tumor cell–blood vessel interactions, and movement of small molecules [120]. Furthermore, it will enable high-throughput screening of large 3D volumes of tumors to detect specific cellular interactions, such as incorporation of labeled cell sub-populations and the initial stage of colonization of a secondary site/organ by metastatic cancer cells. Such kinetic information is vital for understanding the biology of tumors and for optimizing therapeutic approaches.

Currently, most IVM set-ups are bulky bench top devices. The size and bulk of current devices limit their application. However, there is an increasing effort to miniaturize the cameras and microscopes for hand-held use [17,58]. The development of miniaturized endoscopic devices will also allow optical imaging of many interior surfaces of the animal without surgical intervention, and will allow imaging of many other organs and tissues via minimally invasive acute laparoscopy. The prototypes of these microscopes successfully obtained some anatomical and molecular imaging including blood vessel and nerve morphology, calcium transients, reporter gene expression in brain, skin, bladder, liver and colon which are optically accessible with minimum invasion [23,24,81,88-a,98]. In the future, such miniaturized microscopes and/or microendoscopes will become commonplace,

greatly increasing the regions of patients and experimental animals accessible to optical microscopy.

Finally, molecular probes for interrogating various molecular and cellular processes *in vivo* are being actively developed [150,152]. Novel nanocrystal probes in combination with live reporters such as GFP and their variants will allow imaging of multiple events simultaneously (visualized by distinct colors and their combination) [135]. With these improvements in microscopy techniques and probes, IVM will continue to offer new opportunities for unexpected discoveries in tumor biology as well as cancer detection and treatment.

Acknowledgments

This review is based on the following previous review articles: Jain RK, Munn LL, Fukumura D (2002): Dissecting tumor pathophysiology using intravital microscopy. *Nature Reviews Cancer* 2:266–76; Jain RK (2005): Normalization of tumor vasculature: an emerging concept in antiangiogenic therapy. *Science* 307:58–62; Fukumura D (2005): Role of microenvironment on gene expression, angiogenesis and microvascular functions in tumors. In: Meadows GG (ed) "Integration/Interaction of Oncologic Growth." Dordrecht: Springer Science + Business Media B.V., pp. 23–36; Fukumura D and Jain RK (2007): Tumor microenvironment abnormalities: causes, consequences, and strategies to normalize. *Journal of Cellular Biochemistry* 101: 937–949; Fukumura D, Jain RK (2007): Tumor microvasculature and microenvironment: targets for anti-angiogenesis and normalization. *Microvascular Research* 74:72–84; Jain RK, Booth MF, Padera TP, Munn LL, Fukumura D, Brown E (2008): Applications of non-linear intra-vital microscopy in tumor biology In: So P., Masters B. (eds) Handbook of Biological Nonlinear Optical Microscopy. New York, NY: Oxford University Press. Chapter 29. pp. 735–56; Fukumura D, Jain RK (2008): Imaging angiogenesis and the microenvironment. *APMIS* 116: 695–715. The work summarized here has been supported by continuous support from the National Cancer Institute since 1980 including P01-CA-080124 (R.K. Jain and D. Fukumura), R01-CA085140 (R.K. Jain), R01-CA096915 (D. Fukumura), R01-CA115767 (R.K. Jain), R01-CA126642 (R.K. Jain) and R21-139168 (D.G. Duda).

REFERENCES

1. Alexandrakis G, Brown EB, Tong RT, et al. Two-photon fluorescence correlation microscopy reveals the two-phase nature of transport in tumors. Nat Med 2004;10:203–207. [PubMed: 14716306]
2. Baish JW, Jain RK. Fractals and cancer. Cancer Res 2000;60:3683–3688. [PubMed: 10919633]
3. Batchelor TT, Sorensen AG, di Tomaso E, et al. AZD2171, a pan-VEGF receptor tyrosine kinase inhibitor, normalizes tumor vasculature and alleviates edema in glioblastoma patients. Cancer Cell 2007;11:83–95. [PubMed: 17222792]
4. Berk DA, Swartz MA, Leu AJ, Jain RK. Transport in lymphatic capillaries. II. Microscopic velocity measurement with fluorescence photobleaching. Am J Physiol 1996;270:H330–H337. [PubMed: 8769769]
5. Berk DA, Yuan F, Leunig M, Jain RK. Fluorescence Photobleaching with Spatial Fourier-Analysis: Measurement of Diffusion in Light-Scattering Media. Biophys J 1993;65:2428–2436. [PubMed: 8312481]
6. Berk DA, Yuan F, Leunig M, Jain RK. Direct in vivo measurement of targeted binding in a human tumor xenograft. Proceedings of the National Academy of Sciences of the United States of America 1997;94:1785–1790. [PubMed: 9050856]
7. Boissonnas A, Fetler L, Zeelenberg IS, Hugues S, Amigorena S. In vivo imaging of cytotoxic T cell infiltration and elimination of a solid tumor. J Exp Med 2007;204:345–356. [PubMed: 17261634]
8. Brown JM. The hypoxic cell: a target for selective cancer therapy – eighteenth Bruce F. Cain Memorial Award lecture. Cancer Res 1999;59:5863–5870. [PubMed: 10606224]
9. Brown EB, Campbell RB, Tsuzuki Y, et al. In vivo measurement of gene expression, angiogenesis, and physiological function in tumors using multiphoton laser scanning microscopy. Nat Med 2001;7:864–868. [PubMed: 11433354]
10. Brown JM, Giaccia AJ. The unique physiology of solid tumors: opportunities (and problems) for cancer therapy. Cancer Res 1998;58:1408–1416. [PubMed: 9537241]

11. Brown E, McKee TD, di Tomaso E, et al. Dynamic imaging of collagen and its modulation in tumors in vivo using second harmonic generation. Nat Med 2003;9:796–801. [PubMed: 12754503]
12. Carmeliet P, Jain RK. Angiogenesis in cancer and other diseases: from genes to function to therapy. Nature 2000;407:249–257. [PubMed: 11001068]
13. Chambers AF, MacDonald IC, Schmidt EE, et al. Steps in tumor metastasis: new concepts from intravital videomicroscopy. Cancer Metastasis Rev 1995;14:279–301. [PubMed: 8821091]
14. Chang YS, Tomaso Ed, McDonald DM, Jones RC, Jain RK, Munn LL. Mosaic blood vessels in tumors: frequency of cancer cells in contact with flowing blood. Proceedings of the National Academy of Sciences of the United States of America 2000;97:14608–14613. [PubMed: 11121063]
15. Chary SR, Jain RK. Direct measurement of interstitial convection and diffusion of albumin in normal and neoplastic tissues by fluorescence photobleaching. Proceedings of the National Academy of Sciences of the United States of America 1989;86:5385–5389. [PubMed: 2748592]
16. Chishima T, Miyagi Y, Wang X, et al. Cancer invasion and micrometastasis visulaized in live tissue by green fluorescenct protein expression. Cancer Res 1997;57:2042–2047. [PubMed: 9158003]
17. Delaney PM, Harris MR, King RG. Novel microscopy using fibre optic confocal imaging and its suitability for subsurface blood vessel imaging in vivo. Clin Exp Pharmacol Physiol 1993;20:197–198. [PubMed: 8467575]
18. Dellian M, Helmlinger G, Yuan F, Jain RK. Fluorescence ratio imaging and optical sectioning: effect of glucose on spatial and temporal gradients. Br J Cancer 1996;74:1206–1215. [PubMed: 8883406]
19. Dellian M, Witwer BP, Salehi HA, Yuan F, Jain RK. Quantitation and physiological characterization of angiogenic vessels in mice: effect of basic fibroblast growth factor, vascular endothelial growth factor/vascular permeability factor, and host microenvironment. Am J Pathol 1996;149:59–72. [PubMed: 8686763]
20. Detmar M, Brown LF, Schön MP, et al. Increased microvascular density and enhanced leukocyte rolling and adhesion in the skin of VEGF transgenic mice. J Invest Dermatol 1998;111:1–6. [PubMed: 9665379]
21. Dewhirst MW. Concepts of oxygen transport at the microcirculatory level. Semin Radiat Oncol 1998;8:143–150. [PubMed: 9634491]
22. Dewhirst M, Ong E, Braun R, et al. Quantification of longitudinal tissue pO_2 gradients in window chamber tumours: impact on tumor hypoxia. Br J Cancer 1999;79:1717–1722. [PubMed: 10206282]
23. D'Hallewin MA, El Khatib S, Leroux A, Bezdetnaya L, Guillemin F. Endoscopic confocal fluorescence microscopy of normal and tumor bearing rat bladder. J Urol 2005;174:736–740. [PubMed: 16006967]
24. Dickensheets D, Kino G. Micromachined scanning confocal optical microscope. Opt Lett 1996;21:764–766. [PubMed: 19876151]
25. Dintenfass L. Hemorheology of cancer:an example of melanoma. Survival times and abnormality of blood viscosity factors. Clin Hemorheol 1982;2:259–271.
26. Duda DG, Fukumura D, Munn LL, et al. Differential transplantability of tumor-associated stromal cells. Cancer Res 2004;64:5920–5924. [PubMed: 15342367]
27. Dvorak, HF.; Nagy, JA.; Feng, D.; Dvorak, AM. Tumor architecture and targeted delivery. In: Abrams, PG.; Fritzberg, AR., editors. Radioimmunotherapy of Cancer. New York: Marcel Dekker, Inc; 2002. p. 107-135.
28. Egeblad M, Ewald AJ, Askautrud HA, et al. Visualizing stromal cell dynamics in different tumor microenvironments by spinning disk confocal microscopy. Dis Model Mech 2008;1:155–167. [PubMed: 19048079]
29. Elenbaas B, Weinberg RA. Heterotypic signaling between epithelial tumor cells and fibroblasts in carcinoma formation. Exp Cell Res 2001;264:169–184. [PubMed: 11237532]
30. Endrich B, Intaglietta M, Reinhold HS, Gross JF. Hemodynamic characteristics in microcirculatory blood channels during early tumor growth. Cancer Res 1979;39:17–23. [PubMed: 761187]

31. Endrich B, Reinhold HS, Gross JF, Intaglietta M. Tissue perfusion inhomogeneity during early tumor growth in rats. J Natl Cancer Inst 1979;62:387–395. [PubMed: 283271]
32. Erler JT, Bennewith KL, Nicolau M, et al. Lysyl oxidase is essential for hypoxia-induced metastasis. Nature 2006;440:1222–1226. [PubMed: 16642001]
33. Fan GY, Fujisaki H, Miyawaki A, Tsay RK, Tsien RY, Ellisman MH. Video-rate scanning two-photon excitation fluorescence microscopy and ratio imaging with cameleons. Biophys J 1999;76:2412–2420. [PubMed: 10233058]
34. Ferrara N, Alitaro K. Clinical application of angiogenic growth factors and their inhibitors. Nat Med 1999;5:1359–1364. [PubMed: 10581076]
35. Fidler IJ. Angiogenic heterogeneity: regulation of neoplastic angiogenesis by the organ microenvironment. J Natl Cancer Inst 2001;93:1040–1041. [PubMed: 11459857]
36. Folkman, J. Tumor angiogenesis. In: Holland, JF.; Frei, E., III; Bast, RC., Jr, et al., editors. Cancer Medicine. 5th edn. Ontario, Canada: B. C. Decker Inc; 2000. p. 132-152.
37. Fukumura, D. Role of microenvironment on gene expression, angiogenesis and microvascular functions in tumors. In: Meadows, GG., editor. Integration/Interaction of Oncologic Growth. Dordrecht: Springer Science + Business Media B.V.; 2005. p. 23-36.
38. Fukumura D, Jain RK. Tumor microvasculature and microenvironment: targets for anti-angiogenesis and normalization. Microvasc Res 2007;74:72–84. [PubMed: 17560615]
39. Fukumura D, Jain RK. Imaging angiogenesis and the microenvironment. APMIS 2008;116:695–715. [PubMed: 18834413]
40. Fukumura D, Kashiwagi S, Jain RK. Role of nitric oxide in tumour progression. Nat Rev Cancer 2006;6:521–534. [PubMed: 16794635]
41. Fukumura D, Salehi HA, Witwer B, Tuma RF, Melder RJ, Jain RK. Tumor necrosis factor α-induced leukocyte adhesion in normal and tumor vessels: effect of tumor type, transplantation site, and host strain. Cancer Res 1995;55:4824–4829. [PubMed: 7585514]
42. Fukumura D, Ushiyama A, Duda DG, et al. Paracrine regulation of angiogenesis and adipocyte differentiation during in vivo adipogenesis. Circ Res 2003;93:e88–e97. [PubMed: 14525808]
43. Fukumura D, Xavier R, Sugiura T, et al. Tumor induction of VEGF promoter activity in stromal cells. Cell 1998;94:715–725. [PubMed: 9753319]
44. Fukumura D, Xu L, Chen Y, Gohongi T, Seed B, Jain RK. Hypoxia and acidosis independently up-regulate vascular endothelial growth factor transcription in brain tumors in vivo. Cancer Res 2001;61:6020–6024. [PubMed: 11507045]
45. Fukumura D, Yuan F, Endo M, Jain RK. Role of nitric oxide in tumor microcirculation: blood flow, vascular permeability, and leukocyte-endothelial interactions. Am J Pathol 1997;150:713–725. [PubMed: 9033284]
46. Fukumura D, Yuan F, Monsky WL, Chen Y, Jain RK. Effect of host microenvironment on the microcirculation of human colon adenocarcinoma. Am J Pathol 1997;151:679–688. [PubMed: 9284816]
47. Gazit Y, Berk DA, Leunig M, Baxter LT, Jain RK. Scale-invariant behavior and vascular network formation in normal and tumor tissue. Phys Rev Lett 1995;75:2428–2431. [PubMed: 10059301]
48. Gerlowski LE, Jain RK. Microvascular permeability of normal and neoplastic tissues. Microvasc Res 1986;31:288–305. [PubMed: 2423854]
49. Giantonio BJ, Catalano PJ, Meropol NJ, et al. Bevacizumab in combination with oxaliplatin, fluorouracil, and leucovorin (FOLFOX4) for previously treated metastatic colorectal cancer: results from the Eastern Cooperative Oncology Group Study E3200. J Clin Oncol 2007;25:1539–1544. [PubMed: 17442997]
50. Gohongi T, Fukumura D, Boucher Y, et al. Tumor-host interactions in the gallbladder suppress distal angiogenesis and tumor growth: involvement of transforming growth factor β1. Nat Med 1999;5:1203–1208. [PubMed: 10502827]
51. Greenberg JI, Shields DJ, Barillas SG, et al. A role for VEGF as a negative regulator of pericyte function and vessel maturation. Nature 2008;456:809–813. [PubMed: 18997771]
52. Groner W, Winkelman JW, Harris AG, et al. Orthogonal polarization spectral imaging: a new method for study of the microcirculation. Nat Med 1999;5:1209–1213. [PubMed: 10502828]

53. Gutman M, Singh RK, Xie K, Bucana CD, Fidler IJ. Regulation of interleukin-8 expression in human melanoma cells by the organ environment. Cancer Res 1995;55:2470–2475. [PubMed: 7758001]
54. Hagendoorn J, Padera TP, Kashiwagi S, et al. Endothelial nitric oxide synthase regulates microlymphatic flow via collecting lymphatics. Circ Res 2004;95:204–209. [PubMed: 15192027]
55. Hamzah J, Jugold M, Kiessling F, et al. Vascular normalization in Rgs5-deficient tumours promotes immune destruction. Nature 2008;453:410–414. [PubMed: 18418378]
56. Harris AL. Hypoxia: a key regulatory factor in tumour growth. Nature Reviews Cancer 2002;2:38–47.
57. Helmchen F, Denk W. New developments in multiphoton microscopy. Curr Opin Neurobiol 2002;12:593–601. [PubMed: 12367641]
58. Helmchen F, Fee MS, Tank DW, Denk W. A miniature head-mounted two-photon microscope. high-resolution brain imaging in freely moving animals. Neuron 2001;31:903–912. [PubMed: 11580892]
59. Helmlinger G, Yuan F, Dellian M, Jain RK. Interstitial pH and pO_2 gradients in solid tumors in vivo: high-resolution measurements reveal a lack of correlation. Nat Med 1997;3:177–182. [PubMed: 9018236]
60. Hobbs SK, Monsky WL, Yuan F, et al. Regulation of transport pathways in tumor vessels: role of tumor type and host microenvironment. Proceedings of the National Academy of Sciences of the United States of America 1998;95:4607–4612. [PubMed: 9539785]
61. Hoffman RM. Visualization of GFP-expressing tumors and metastasis in vivo. BioTechniques 2001;30:1016–1026. [PubMed: 11355337]
62. Hoshida T, Isaka N, Hagendoorn J, et al. Imaging steps of lymphatic metastasis reveals that vascular endothelial growth factor-C increases metastasis by increasing delivery of cancer cells to lymph nodes: therapeutic implications. Cancer Res 2006;66:8065–8075. [PubMed: 16912183]
63. Huang P, McKee TD, Jain RK, Fukumura D. Green fluorescent protein (GFP)-expressing tumor model derived from a spontaneous osteosarcoma in a vascular endothelial growth factor (VEGF)-GFP transgenic mouse. Comp Med 2005;55:236–243. [PubMed: 16089171]
64. Huber PE, Bischof M, Jenne J, et al. Trimodal cancer treatment: beneficial effects of combined antiangiogenesis,radiation, and chemotherapy. Cancer Res 2005;65:3643–3655. [PubMed: 15867359]
65. Hurwitz H, Fehrenbacher L, Novotny W, et al. Bevacizumab plus irinotecan, fluorouracil, and leucovorin for metastatic colorectal cancer. N Engl J Med 2004;350:2335–2342. [PubMed: 15175435]
66. Isaka N, Padera TP, Hagendoorn J, Fukumura D, Jain RK. Peritumor lymphatics induced by vascular endothelial growth factor-C exhibit abnormal function. Cancer Res 2004;64:4400–4404. [PubMed: 15231646]
67. Izumi Y, Xu L, diTomaso E, Fukumura D, Jain RK. Herceptin acts as an anti-angiogenic cocktail. Nature 2002;416:279–280. [PubMed: 11907566]
68. Jain RK. Determinants of tumor blood flow: a review. Cancer Res 1988;48:2641–2658. [PubMed: 3282647]
69. Jain RK. Barriers to drug delivery in solid tumors. Sci Am 1994;271:58–65. [PubMed: 8066425]
70. Jain RK. The Eugene M. Landis Award Lecture. Delivery of molecular and cellular medicine to solid tumors. Microcirculation 1997;4:1–23. [PubMed: 9110280]
71. Jain RK. Normalization of tumor vasculature: an emerging concept in antiangiogenic therapy. Science 2005;307:58–62. [PubMed: 15637262]
72. Jain, RK.; Booth, MF.; Padera, TP.; Munn, LL.; Fukumura, D.; Brown, E. Applications of non-linear intravital microscopy in tumor biology. In: So, P.; Masters, B., editors. Handbook of Biological Nonlinear Optical Microscopy. New York: Oxford University Press; 2008. p. 735-756.
73. Jain RK, Duda DG, Clark JW, Loeffler JS. Lessons from phase III clinical trials on anti-VEGF therapy for cancer. Nat Clin Pract Oncol 2006;3:24–40. [PubMed: 16407877]
74. Jain RK, Fenton BT. Intra-tumor lymphatic vessels: a case of mistaken identity or malfunction. J Natl Cancer Inst 2002;94:417–421. [PubMed: 11904313]

75. Jain RK, Koenig GC, Dellian M, Fukumura D, Munn LL, Melder RJ. Leukocyte-endothelial adhesion and angiogenesis in tumors. Cancer Metastasis Rev 1996;15:195–204. [PubMed: 8842491]
76. Jain RK, Munn LL, Fukumura D. Dissecting tumor pathophysiology using intravital microscopy. Nature Reviews Cancer 2002;2:266–276.
77. Jain, RK.; Munn, LL.; Fukumura, D.; Melder, RJ. In vitro and in vivo quaqntification of adhesion between leukocytes and vascular endothelium. In: Morgan, JR.; Yarmush, ML., editors. Methods in Molecular Medicine, Vol. 18: Tissue Engineering Methods and Protocols. Totowa: Humana Press Inc; 1998. p. 553-575.
78. Jain RK, Safabakhsh N, Sckell A, et al. Endothelial cell death, angiogenesis, and microvascular function after castration in an androgendependent tumor: role of vascular endothelial growth factor. Proceedings of the National Academy of Sciences of the United States of America 1998;95:10820–10825. [PubMed: 9724788]
79. Jain RK, Tong R, Munn LL. Effect of vascular normalization by antiangiogenic therapy on inerstitial hypertension, peritumor edema, and lymphatic metastasis: insighs from a mathematical model. Cancer Res 2007;67:2729–2735. [PubMed: 17363594]
80. Jeltsch M, Kaipainen A, Joukov V, et al. Hyperplasia of lymphatic vessels in VEGF-C transgenic mice. Science 1997;276:1423–1425. [PubMed: 9162011]
81. Jung JC, Mehta AD, Aksay E, Stepnoski R, Schnitzer MJ. In vivo mammalian brain imaging using one- and two-photon fluorescence microendoscopy. J Neurophysiol 2004;92:3121–3133. [PubMed: 15128753]
82. Kadambi A, Carreira CM, Yun C, et al. Vascular endothelial growth factor (VEGF)-C differentially affects tumor vascular function and leukocyte recruitment: role of VEGF-receptor 2 and host VEGF-A. Cancer Res 2001;61:2404–2408. [PubMed: 11289105]
83. Kamoun WS, Ley CD, Farrar CT, et al. Edema control by cediranib, a vascular endothelial growth factor receptor-targeted kinase inhibitor, prolongs survival despite persistent brain tumor growth in mice. J Clin Oncol 2009;27:2542–2552. [PubMed: 19332720]
84. Kashiwagi S, Izumi Y, Gohongi T, et al. NO mediates mural cell recruitment and vessel morphogenesis in murine melanomas and tissue-engineered blood vessels. J Clin Invest 2005;115:1816–1827. [PubMed: 15951843]
85. Kashiwagi S, Tsukada K, Xu L, et al. Peri-vascular nitric oxide gradients normalize tumor vasculature. Nat Med 2008;14:255–257. [PubMed: 18278052]
86. Kerbel RS. Tumor angiogenesis: past, present and the near future. Carcinogenesis 2000;21:505–515. [PubMed: 10688871]
87. Kim KH, Buehler C, So PTC. High-speed, two-photon scanning microscope. Appl Opt 1999;38:6004–6009. [PubMed: 18324120]
88. Kim I, Moon S-O, Park SK, Chae SW, Koh GY. Angiopoietin-1 reduces VEGF-stimulated leukocyte adhesion to endothelial cells by reducing ICAM-1, VCAM-1, and E-selectin expression. Circ Res 2010;89:477–479. [PubMed: 11557733]
88-a. Kim P, Chung E, Hiroshi Yamashit H, Hung KE, Mizoguchi A, Kucherlapati R, Dai Fukumura D, Jain RK, Yun SH. *In vivo* wide-area cellular imaging by side-view endomicroscopy. Nature Methods. 2010 in press.
89. Kimura H, Braun R, Ong E, et al. Fluctuations in red cell flux in tumor microvessels can lead to transient hyoxia and reoxygenation in tumor parenchyma. Cancer Res 1996;56:5522–5528. [PubMed: 8968110]
90. Kleinfeld D, Mitra PP, Helmchen F, Denk W. Fluctuations and stimulus-induced changes in blood flow observed in individual capillaries in layers 2 through 4 of rat neocortex. Proceedings of the National Academy of Sciences of the United States of America 1998;95:15741–15746. [PubMed: 9861040]
91. Koike N, Fukumura D, Gralla O, Au P, Schechner JS, Jain RK. Tissue engineering: creation of long-lasting blood vessels. Nature 2004;428:138–139. [PubMed: 15014486]
92. Kozin SV, Boucher Y, Hicklin DJ, Bohlen P, Jain RK, Suit HD. Vascular endothelial growth factor receptor-2-blocking antibody potentiates radiation-induced long-term control of human tumor xenografts. Cancer Res 2001;61:39–44. [PubMed: 11196192]

93. Lee CG, Heijn M, di Tomaso E, et al. Anti-vascular endothelial growth factor treatment augments tumor radiation response under normoxic or hypoxic conditions. Cancer Res 2000;60:5565–5570. [PubMed: 11034104]
94. Lendvai B, Stern EA, Chen B, Svoboda K. Experience-dependent plasticity of dendritic spines in the developing rat barrel cortex in vivo. Nature 2000;404:876–881. [PubMed: 10786794]
95. Leu AJ, Berk DA, Lymboussaki A, Alitalo K, Jain RK. Absence of functional lymphatics within a murine sarcoma: a molecular and functional evaluation. Cancer Res 2000;60:4324–4327. [PubMed: 10969769]
96. Leu AJ, Berk DA, Yuan F, Jain RK. Flow velocity in the superficial lymphatic network of the mouse tail. Am J Physiol 1994;267:H1507–H1513. [PubMed: 7943396]
97. Leunig M, Yuan F, Menger MD, et al. Angiogenesis, microvascular architecture, microhemodynamics, and interstitial fluid pressure during early growth of human adenocarcinoma LS174T in SCID mice. Cancer Res 1992;52:6553–6560. [PubMed: 1384965]
98. Levene MJ, Dombeck DA, Kasischke KA, Molloy RP, Webb WW. In vivo multiphoton microscopy of deep brain tissue. J Neurophysiol 2004;91:1908–1912. [PubMed: 14668300]
99. Li G, Satyamoorthy K, Meier F, Berking C, Bogenrieder T, Herlyn M. Function and regulation of melanoma–stromal fibroblast interactions: when seeds meet soil. Oncogene 2003;22:3162–3171. [PubMed: 12789292]
100. Li C-Y, Shan S, Huang Q, et al. Initial stages of tumor cell-induced angiogenesis: evaluation via skin window chambers in rodent models. J Natl Cancer Inst 2000;92:143–147. [PubMed: 10639516]
101. Lichtenbeld HC, Ferarra N, Jain RK, Munn LL. Effect of local anti-VEGF antibody treatment on tumor microvessel permeability. Microvasc Res 1999;57:357–362. [PubMed: 10329263]
102. Lichtenbeld HC, Yuan F, Michel CC, Jain RK. Perfusion of single tumor microvessels: application to vascular permeability measurement. Microcirculation 1996;3:349–357. [PubMed: 9086446]
103. Liotta LA, Kohn EC. The microenvironment of the tumour–host interface. Nature 2001;411:375–379. [PubMed: 11357145]
104. MacDonald IC, Groom AC, Chambers AF. Cancer spread and micrometastasis development: quantitative approaches for in vivo models. Bioessays 2002;24:885–893. [PubMed: 12325121]
105. Martin GR, Jain RK. Fluorescence ratio imaging measurement of pH gradients: calibration and application in normal and tumor tissues. Microvasc Res 1993;46:216–230. [PubMed: 8246820]
106. Martin GR, Jain RK. Noninvasive measurement of interstitial pH profiles in normal and neoplastic tissue using fluorescence ratio imaging microscopy. Cancer Res 1994;54:5670–5674. [PubMed: 7923215]
107. Mazzone M, Dettori D, Leite de Oliveira R, et al. Heterozygous deficiency of PHD2 restores tumor oxygenation and inhibits metastasis via endothelial normalization. Cell 2009;136:839–851. [PubMed: 19217150]
108. McDonald DM, Choyke PL. Imaging of angiogenesis: from microscope to clinic. Nat Med 2003;9:713–725. [PubMed: 12778170]
109. Melder RJ, Koenig GC, Witwer BP, Safabakhsh N, Munn LL, Jain RK. During angiogenesis, vascular endothelial growth factor and basic fibroblast growth factor regulate natural killer cell adhesion to tumor endothelium. Nat Med 1996;2:992–997. [PubMed: 8782456]
110. Melder RJ, Salehi HA, Jain RK. Interaction of activated natural killer cells with normal and tumor vessels in cranial windows in mice. Microvasc Res 1995;50:35–44. [PubMed: 7476578]
111. Monsky WL, Carreira CM, Tsuzuki Y, Gohongi T, Fukumura D, Jain RK. Role of host microenvironment in angiogenesis and microvascular functions in human breast cancer xenografts: mammary fat pad vs. cranial tumors. Clin Cancer Res 2002;8:1008–1013. [PubMed: 11948107]
112. Monsky WL, Fukumura D, Gohongi T, et al. Augmentation of transvascular transport of macromolecules and nanoparticles in tumors using vascular endothelial growth factor. Cancer Res 1999;59:4129–4135. [PubMed: 10463618]
113. Nagy JA, Vasile E, Feng D, et al. Vascular permeability factor/vascular endothelial growth factor induces lymphangiogenesis as well as angiogenesis. J Exp Med 2002;196:1497–1506. [PubMed: 12461084]

114. Naumov GN. Persistence of solitary mammary carcinoma cells in a secondary site: a possible contribution to dormancy. Cancer Res 2002;62:2162–2168. [PubMed: 11929839]
115. Naumov GN, Wilson SM, MacDonald IC, et al. Cellular expression of green fluorescent protein, coupled with high-resolution in vivo videomicroscopy, to monitor steps in tumor metastasis. J Cell Sci 1999;112:1835–1842. [PubMed: 10341203]
116. Niesner R, Andresen V, Neumann J, Spiecker H, Gunzer M. The power of single and multibeam two-photon microscopy for high-resolution and high-speed deep tissue and intravital imaging. Biophys J 2007;93:2519–2529. [PubMed: 17557785]
117. Ny A, Koch M, Schneider M, et al. A genetic Xenopus laevis tadpole model to study lymphangiogenesis. Nat Med 2005;11:998–1004. [PubMed: 16116431]
118. Ohkubo C, Bigos D, Jain RK. Interleukin 2 induced leukocyte adhesion to the normal and tumor microvascular endothelium in vivo and its inhibition by dextran sulfate: implications for vascular leak syndrome. Cancer Res 1991;51:1561–1563. [PubMed: 1997196]
119. Padera TP, Kadambi A, di Tomaso E, et al. Lymphatic metastasis in the absence of functional intratumor lymphatics. Science 2002;296:1883–1886. [PubMed: 11976409]
120. Padera TP, Stoll BR, So PTC, Jain RK. High-speed intravital multiphoton laser scanning microscopy of microvasculature, lymphatics, and leukocyte–endothelial interactions. Mol Imaging 2002;1:9–15. [PubMed: 12920856]
121. Padera TP, Stoll BR, Tooredman JB, Capen D, di Tomaso E, Jain RK. Pathology: cancer cells compress intratumour vessels. Nature 2004;427:695. [PubMed: 14973470]
122. Pennacchietti S, Michieli P, Galluzzo M, Mazzone M, Giordano S, Comoglio PM. Hypoxia promotes invasive growth by transcriptional activation of the met protooncogene. Cancer Cell 2003;3:347–361. [PubMed: 12726861]
123. Perentes JY, Duda DG, Jain RK. Visualizing anti-tumor immune responses in vivo. Dis Model Mech 2009;2:107–110. [PubMed: 19259379]
124. Perentes JY, McKee TD, Ley CD, et al. In vivo imaging of extracellular matrix remodeling by tumor-associated fibroblasts. Nat Methods 2009;6:143–145. [PubMed: 19151720]
125. Pollard JW. Tumour-educated macrophages promote tumour progression and metastasis. Nat rev Cancer 2004;4:71–78. [PubMed: 14708027]
126. Roessel, Pv; Brand, AH. Imaging into the future: visualizing gene expression and protein interactions with fluorescent proteins. Nat Cell Biol 2002;4:E15–E20. [PubMed: 11780139]
127. Rofstad EK, Mathiesen B, Kindem K, Galappathi K. Acidic extracellular pH promotes experimental metastasis of human melanoma cells in athymic nude mice. Cancer Res 2006;66:6699–6707. [PubMed: 16818644]
128. Roose T, Netti PA, Munn LL, Boucher Y, Jain RK. Solid stress generated by spheroid growth estimated using a linear poroelasticity model. Microvasc Res 2003;66:204–212. [PubMed: 14609526]
129. Ruiter DJ, van Krieken JH, van Muijen GN, de Waal RM. Tumour metastasis: is tissue an issue? Lancet Oncology 2001;2:109–112. [PubMed: 11905791]
130. Sandler A, Gray R, Perry MC, et al. Paclitaxel-carboplatin alone or with bevacizumab for non-small-cell lung cancer. N Engl J Med 2006;355:2542–2550. [PubMed: 17167137]
131. Sasaki A, Melder RJ, Whiteside TL, Herberman RB, Jain RK. Preferential localization of human adherent lymphokine-activated killer cells in tumor microcirculation. J Natl Cancer Inst 1991;83:433–437. [PubMed: 1999850]
132. Shu X, Royant A, Lin MZ, et al. Mammalian expression of infrared fluorescent proteins engineered from a bacterial phytochrome. Science 2009;324:804–807. [PubMed: 19423828]
133. Sorensen AG, Batchelor TT, Zhang WT, et al. A “vascular normalization index” as potential mechanistic biomarker to predict survival after a single dose of cediranib in recurrent glioblastoma patients. Cancer Res 2009;69:5296–5300. [PubMed: 19549889]
134. Stockmann C, Doedens A, Weidemann A, et al. Deletion of vascular endothelial growth factor in myeloid cells accelerates tumorigenesis. Nature 2008;456:814–818. [PubMed: 18997773]
135. Stroh M, Zimmer JP, Duda DG, et al. Quantum dots spectrally distinguish multiple species within the tumor milieu in vivo. Nat Med 2005;11:678–682. [PubMed: 15880117]

136. Swartz MA, Berk DA, Jain RK. Transport in lymphatic capillaries. I. Macroscopic measurements using residence time distribution theory. Am J Physiol 1996;270:H324–H329. [PubMed: 8769768]

137. Tam J, Duda DG, Perentes JY, Quadri RS, Fukumura D, Jain RK. Blockade of VEGFR2 and not VEGFR1 can limit diet-induced fat tissue expansion: role of local versus bone marrowderived endothelial cells. PLoS ONE 2009;4:e4974. [PubMed: 19333381]

138. Tatum JL, Kelloff GJ, Gillies RJ, et al. Hypoxia: importance in tumor biology, noninvasive measurement by imaging, and value of its measurement in the management of cancer therapy. Int J Radiat Biol 2006;82:699–757. [PubMed: 17118889]

139. Thomas MW, Grichnik JM, Izatt JA. Three-dimensional images and vessel rendering using optical coherence tomography. Arch Dermatol 2007;143:1468–1469. [PubMed: 18025387]

140. Ting AY, Kain KH, Klemke RL, Tsien RY. Genetically encoded fluorescent reporters of protein tyrosine kinase activities in living cells. Proceedings of the National Academy of Sciences of the United States of America 2001;98:15003–15008. [PubMed: 11752449]

141. Tlsty TD. Stromal cells can contribute oncogenic signals. Cancer Biology 2001;11:97–104.

142. di, Tomaso E.; Capen, D.; Haskell, A., et al. Mosaic tumor vessels: cellular basis and ultrastructure of focal regions lacking endothelial cell markers. Cancer Res 2005;65:5740–5749. [PubMed: 15994949]

143. Tong RT, Boucher Y, Kozin SV, Winkler F, Hicklin DJ, Jain RK. Vascular normalization by vascular endothelial growth factor receptor 2 blockade induces a pressure gradient across the vasculature and improves drug penetration in tumors. Cancer Res 2004;64:3731–3736. [PubMed: 15172975]

144. Torres-Filho IP, Leunig M, Yuan F, Intaglietta M, Jain RK. Noninvasive measurement of microvascular and interstitial oxygen profiles in a human tumor in SCID mice. Proceedings of the National Academy of Sciences of the United States of America 1994;91:2081–2085. [PubMed: 8134352]

145. Tredan O, Galmarini CM, Patel K, Tannock IF. Drug resistance and the solid tumor microenvironment. J Natl Cancer Inst 2007;99:1441–1454. [PubMed: 17895480]

146. Tsuzuki Y, Carreira CM, Bockhorn M, Xu L, Jain RK, Fukumura D. Pancreas microenvironment promotes VEGF expression and tumor growth: novel window models for pancreatic tumor angiogenesis and microcirculation. Lab Invest 2001;81:1439–1452. [PubMed: 11598156]

147. Tsuzuki Y, Fukumura D, Oosthuyse B, Koike C, Carmeliet P, Jain RK. Vascular endothelial growth factor (VEGF) modulation by targeting hypoxia inducible factor-1α → Hypoxia response element → VEGF cascade differentially regulates vascular response and growth rate in tumors. Cancer Res 2000;60:6248–6252. [PubMed: 11103778]

148. Vakoc BJ, Lanning RM, Tyrrell JA, et al. Three-dimensional microscopy of the tumor microenvironment in vivo using optical frequency domain imaging. Nat Med 2009;15:1219–1223. [PubMed: 19749772]

149. Weinberg, RA. The Biology of Cancer. New York: Garland Science Publishing; 2006.

150. Weissleder R. A clearer vision for *in vivo* imaging. Nat Biotechnol 2001;19:316–317. [PubMed: 11283581]

151. Weissleder R. Scaling down imaging: molecular mapping of cancer in mice. Nat Rev Cancer 2002;2:11–18. [PubMed: 11902581]

152. Weissleder R, Ntziachristos V. Shedding light onto live molecular targets. Nat Med 2003;9:123–128. [PubMed: 12514725]

153. Wildiers H, Guetens G, De Boeck G, et al. Effect of antivascular endothelial growth factor treatment on the intratumoral uptake of CPT-11. Br J Cancer 2003;88:1979–1986. [PubMed: 12799646]

154. Willett CG, Boucher Y, di Tomaso E, et al. Direct evidence that the anti-VEGF antibody Bevacizumab has anti-vascular effects in human rectal cancer. Nat Med 2004;10:145–147. [PubMed: 14745444]

155. Willett CG, Duda DG, di Tomaso E, et al. Efficacy, safety, and biomarkers of neoadjuvant bevacizumab, radiation therapy, and Fluorouracil in rectal cancer: a multidisciplinary phase II study. J Clin Oncol 2009;27:3020–3026. [PubMed: 19470921]

156. Winkler F, Kozin SV, Tong R, et al. Kinetics of vascular normalization by VEGFR2 blockade governs brain tumor response to radiation: role of oxygenation, angiopoietin-1 and matrix metalloproteinases. Cancer Cell 2004;6:553–563. [PubMed: 15607960]

157. Wu NZ, Klitzman B, Dodge R, Dewhirst MW. Diminished leukocyte–endothelium interaction in tumor microvessels. Cancer Res 1992;52:4265–4268. [PubMed: 1638539]

158. Wyckoff JB, Segall JE, Condeelis JS. The collection of the motile population of cells from a living tumor. Cancer Res 2000;60:5401–5404. [PubMed: 11034079]

159. Wyckoff JB, Wang Y, Lin EY, et al. Direct visualization of macrophage-assisted tumor cell intravasation in mammary tumors. Cancer Res 2007;67:2649–2656. [PubMed: 17363585]

160. Xu L, Fukumura D, Jain RK. Acidic extracellular pH induces vascular endothelial growth factor (VEGF) in human glioblastoma cells via ERK1/2 MAPK signaling pathway – mechanism of low pH-induced VEGF. J Biol Chem 2002;277:11368–11374. [PubMed: 11741977]

161. Xue C, Wyckoff J, Liang F, et al. Epidermal growth factor receptor overexpression results in increased tumor cell motility in vivo coordinately with enhanced intravasation and metastasis. Cancer Res 2006;66:192–197. [PubMed: 16397232]

162. Yuan F, Chen Y, Dellian M, Safabakhsh N, Ferrara N, Jain RK. Time-dependent vascular regression and permeability changes in established human tumor xenografts induced by an anti-vascular endothelial growth factor/vascular permeability factor antibody. Proceedings of the National Academy of Sciences of the United States of America 1996;93:14765–14770. [PubMed: 8962129]

163. Yuan F, Dellian M, Fukumura D, et al. Vascular permeability in a human tumor xenograft: molecular size dependence and cutoff size. Cancer Res 1995;55:3752–3756. [PubMed: 7641188]

164. Yuan F, Leunig M, Berk DA, Jain RK. Microvascular permeability of albumin, vascular surface area, and vascular volume measured in human adenocarcinoma LS174T using dorsal chamber in SCID mice. Microvasc Res 1993;45:269–289. [PubMed: 8321142]

165. Yuan F, Leunig M, Huang SK, Berk DA, Papahadjopoulos D, Jain RK. Microvascular permeability and interstitial penetration of sterically stabilized (stealth) liposomes in a human tumor xenograft. Cancer Res 1994;54:3352–3356. [PubMed: 8012948]

166. Yuan F, Salehi HA, Boucher Y, Vasthare US, Tuma RF, Jain RK. Vascular permeability and microcirculation of gliomas and mammary carcinomas transplanted in rat and mouse cranial window. Cancer Res 1994;54:4564–4568. [PubMed: 8062241]

167. Zhang H, Issekutz AC. Growth factor regulation of neutrophil-endothelial cell interactions. J Leukoc Biol 2001;70:225–232. [PubMed: 11493614]

168. Zhang J, Ma Y, Taylor SS, Tsien RY. Genetically encoded reporters of protein kinase A activity reveal impact of substrate tethering. Proceedings of the National Academy of Sciences of the United States of America 2001;98:14997–15002. [PubMed: 11752448]

169. Zhu AX, Sahani DV, Duda DG, et al. Efficacy, safety, and potential biomarkers of sunitinib monotherapy in advanced hepatocellular carcinoma: a phase II study. J Clin Oncol 2009;27:3027–3035. [PubMed: 19470923]

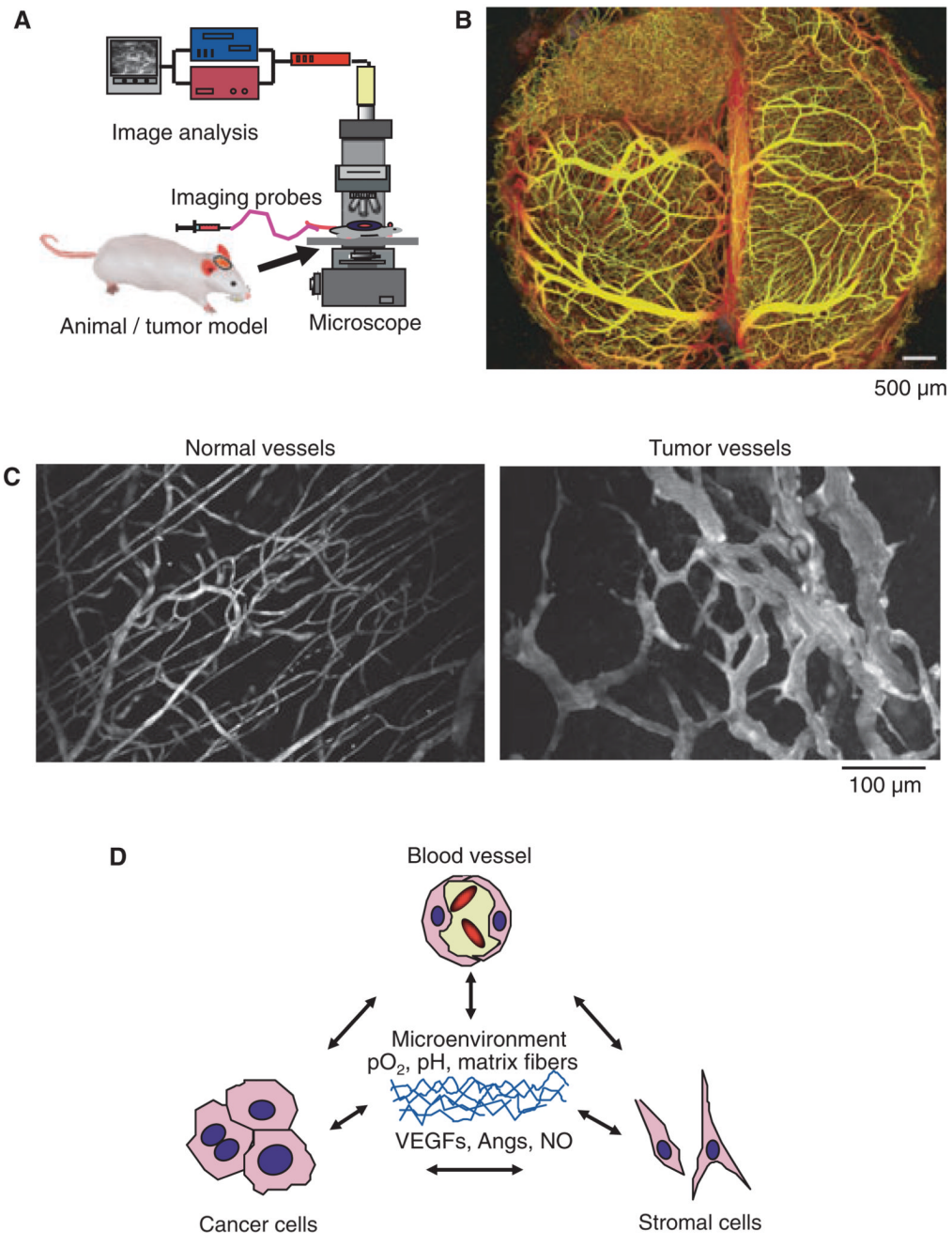

Figure 1.

Imaging of tumor microvasculature and microenvironment. (**A**) Schematic of intravital microscopy set-up. An appropriate animal/tumor model, imaging probe(s), microscope, and image acquisition and analysis system are essential requirement of intravital microscopy. (**B**) OFDI angiography of mouse brain harboring U87 human glioma xenograft showing the depth-projected vasculature within the first 2 mm of mouse brain and tumor (upper left). Depth variation is denoted by color: yellow (superficial) to red (deep). Scale bar, 500 μm. (**C**) Multiphoton laser-scanning microscopy images of normal blood vessels (left) and tumor vessels in LS174T human colon cancer xenografts (right) in mouse dorsal skin chambers. Blood vessels are contrast enhanced by FITC-dextran. The bar indicates 100 μm. (**D**)

Schematic of the composition of solid tumor. Tumors consist not only of cancer cells but also of host stromal cells—non-malignant cells in tumors which include endothelial cells, peri-vascular cells, fibroblasts, and multiple immune cell types. These cells, embedded within a protein-rich extracellular matrix, face a hostile metabolic microenvironment characterized by hypoxia and acidosis. Each of these cells is capable of producing positive and negative regulators of angiogenesis such as vascular endothelial growth factors (VEGFs); angiopoietins (Angs) and nitric oxide (NO) in response to the exposed microenvironment. These local interactions vary with tumor type and site of tumor growth (host organ), and may change during the course of tumor growth and treatment. **B**: reproduced from [148]; **C**: courtesy of Dr. Edward Brown; **D**: reproduced from ref. [37].

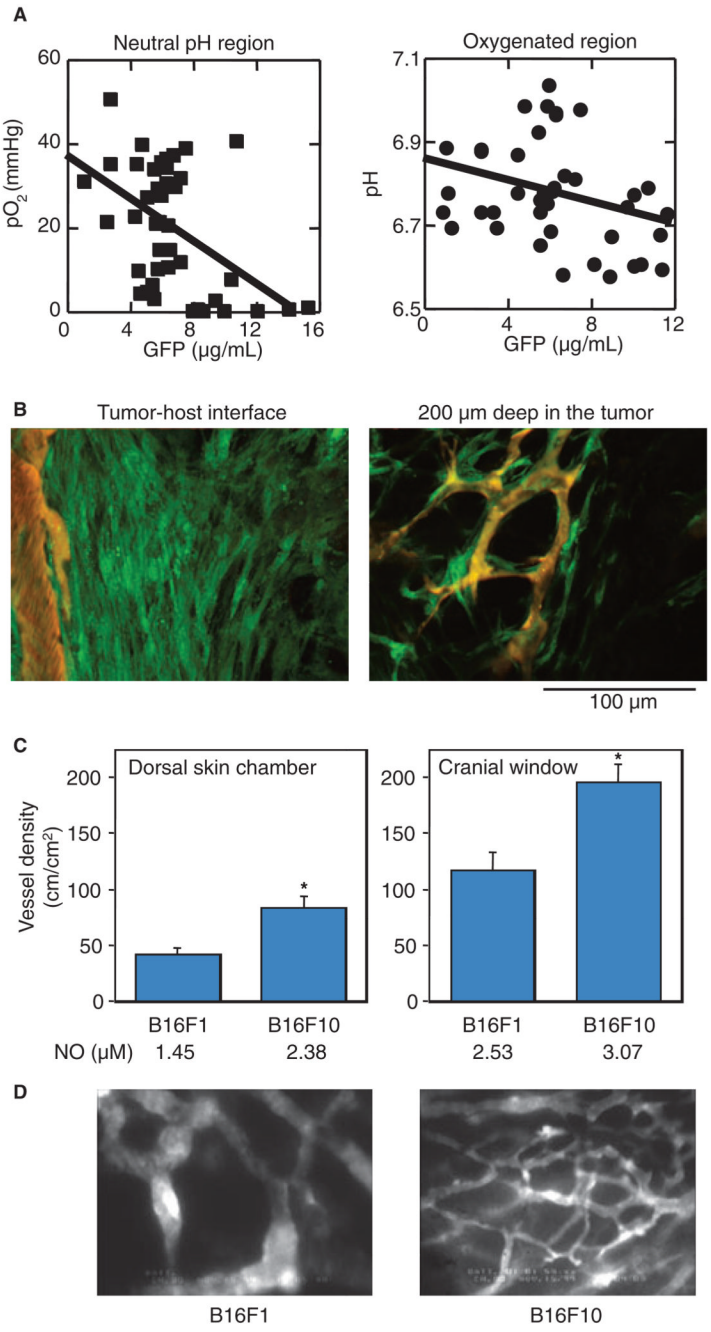

Figure 2.

Regulation of angiogenesis by tumor microenvironment. (**A**) Relationship between VEGF promoter activity and local pO_2 or pH in U87 glioma xenografts. Tumor cell VEGF promoter activity was determined by the intensity of GFP (which is driven by the VEGF promoter). Tissue pO_2 and pH were determined by phosphorescence quenching microscopy with a porphyrin probe and fluorescence ratio-imaging microscopy with BCECF, respectively. Tissue pO_2 level inversely correlated with VEGF promoter activity especially in the region with neutral pH (left) and hypoxic region (not shown). On the other hand, tissue pH level inversely correlated with VEGF promoter activity in the oxygenated area (right). (**B**) Imaging of VEGF promoter activity in host stromal cells: MCaIV murine breast

cancer grown in the dorsal skin chamber of a transgenic mouse expressing GFP under the control of VEGF promoter. Left: high density of activated fibroblasts exhibiting strong VEGF promoter activity (in green) at the host-tumor interface. Blood vessels are contrast enhanced by tetramethylrhodamine-dextran. Right: in contrast, deeper (200 μm) inside the tumor the VEGF expressing host stromal cells (in green) closely associate with blood vessels (in red). The bar indicates 100 μm. (**C**) Angiogenesis and tissue NO level in B16F1 and F10 tumors grown in the dorsal skin chamber and the cranial window. Vessel density was determined by intravital microscopy and tissue NO level was measured by an NO sensitive recessed microelectrode. (**D**) Microangiography of B16F1 and F10 murine melanomas grown in the cranial window. **A**: adapted from ref. [44]; **B**, adapted from ref. [9]; **C, D**: adapted from ref. [84].

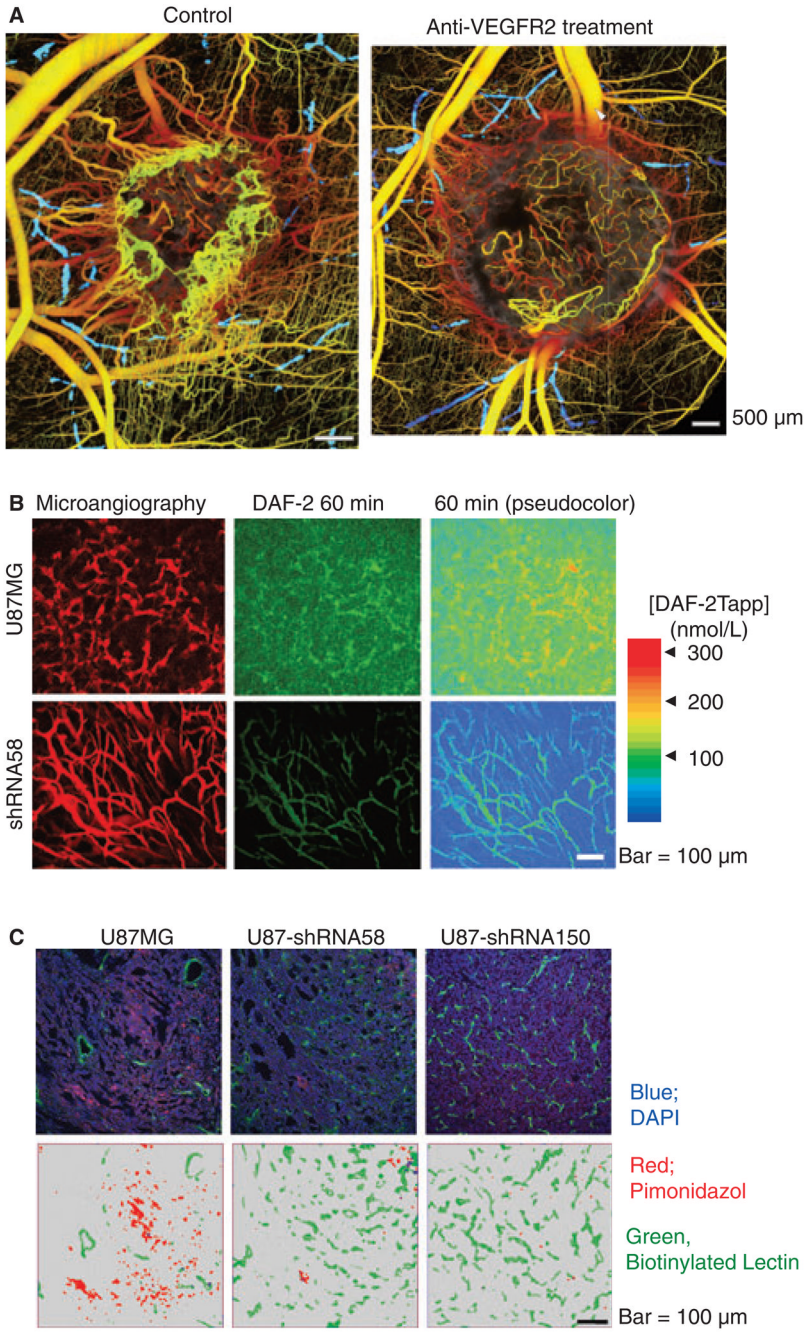

Figure 3.

Imaging therapeutic responses. (**A**) Simultaneous OFDI angiography and lymphangiography of control IgG and anti-VEGFR2 antibody treated MCaIV murine tumors. The images are taken 5 days after the initiation of treatment. For angiography depth-projected images are shown and the depth is denoted by color: yellow (superficial) to red (deep). The lymphatic vascular networks are presented (blue) for both tumors. The bar indicates 500 μm. (**B, C**) Normalization of U87 tumor vasculature by restoration of perivascular NO gradients. Tissue distribution of NO in U87 tumors grown in the cranial window was visualized by means of DAF-2T fluorescence imaging using MPLSM (B). The NO-sensitive fluorescence probe DAF-2 is converted to DAF-2T in the presence of NO, increasing fluorescence by a factor

of 200. Control U87 tumors are shown in top row and *nNOS*-shRNA58-transfected-U87 tumors are shown in bottom row. Left: microangiography using tetramethylrhodamine-dextran (MW 2000 kDa). Middle: representative image of DAF-2T microfluorography captured 60 min after the loading of DAF-2 in tumors. Right: pseudocolor representation of DAF-2T microfluorographs. Color bar in the right shows calibration of the fluorescence intensity with known concentrations of DAF-2T. The bar indicates 100 μm. (**C**) Effects of nNOS silencing in U87 tumor cells on tumor tissue oxygenation. Top row: confocal laser-scanning microscopy images of hypoxyprobe-1 pimonidazole adduct–stained hypoxic cells (in red), lectin-bound perfused blood vessels (in green) and DAPI-stained nuclei (in blue). Bottom row: binarized images of blood vessels (in green) and hypoxic cells (in red). Scale bar, 100 μm. **A**, reproduced from ref. [148]; **B, C**: reproduced from ref. [85].

Table 1

Examples of parameters measured and probes used in intravital microscopy

Parameter	Molecular probe	Reference
Molecular imaging		
Micro-pharmacokinetics	FITC-antibody, TMR-liposome	[6,165]
Microenvironment (pH, pO_2, NO)	BCECF, BSA-porphyrin, DAF-2	[22,59,84,85,106,144]
Enzyme activity (cathepsin B, protein kinase A, tyrosine kinase)	NIRF probe-graft copolymer, CFP-14-3-3τ-YFP reporter gene	[140,151,168]
Gene expression	GFP reporter gene	[9,26,43,44,63,126]
Cellular imaging		
Tracking cancer cells	GFP, calcein, fluorescent nanosphere	[13,14,16,61,62,100, 114,115,158]
Tracking leukocytes	Rhodamine 6G, calcein	[9,41,75,118,157]
Tracking other cells	GFP, nanocrystals	[9,42,85,91,135]
Anatomical imaging		
Tumor size	Endogenous contrast, GFP, OCT, OFDI	[61,97,148]
Vascular architecture (diameter, length, surface area, volume, branching patterns)	Endogenous contrast, OPS, fluorescent-dextran, nanocrystals, OFDI	[52,97,135,148,162,166]
Pore size	TMR-liposome/microsphere with varying size	[60,112]
Lymphatic architecture (diameter, length, branching patterns, valves)	Fluorescent-dextran, nanocrystals, OFDI	[4,62,66,96,117,119,120,148]
Extracellular matrix	Second harmonic generation (type I collagen)	[11]
Tissue viability	OFDI	[148]
Functional imaging		
Blood flow rate	Fluorescent-dextran, RBC (fluorescent, endogenous contrast), OCT	[9,30,31,89,97]
Lymph flow rate	FITC-dextran	[62,136]
Vascular permeability	TMR/Cy5-BSA, nanoparticles, nanocrystals	[9,48,102,135,164]
Interstitial diffusion, convection, and binding	Fluorescent BSA, IgG, dextran, liposomes, nanoparticles	[1,6,15]

FITC, fluorescein isothiocyanate; TMR, tetremethylrhodamine; BCECF, 2′,7′-bis-(2-carboxyethyl)-5,6-carboxyfluorescein; BSA, bovine serum albumine; porphyrin, palladium meso-tetra(4-carboxyphenyl)porphyrin; NIRF, near-infrared fluorescence; CFP, cyan fluorescent protein; 14-3-3τ, phosphoamino acid binding domain; YFP, yellow fluorescent protein; GFP, green fluorescent protein; OCT, optical coherence tomography; OFDI, optical frequency domain imaging; VEGFp, vascular endothelial growth factor promoter; OPS, orthogonal polarization spectral. This table is adapted and updated from ref. [39,76].